Design and fabrication of a miniaturized bulk acoustic filter by high aspect ratio etching

Chung-Hsien Lin
National Tsing Hua University
Power Mechanical Engineering Department
Hsinchu, Taiwan

Hong-Ren Chen
Asia Pacific Microsystems, Incorporated
Hsinchu, Taiwan

Weileun Fang
National Tsing Hua University
Power Mechanical Engineering Department
Hsinchu, Taiwan
E-mail: fang@pme.nthu.edu.tw

Abstract. A 2.45-GHz filter is fabricated by thin film bulk acoustic wave resonator (FBAR) technology. It is designed to minimize die size and simplify the fabrication process simultaneously by using inductive coupling plasma etching. The quality factor of a fabricated single resonator is 1567 and the electromechanical coupling coefficient is 5.7%. The fabricated filter has minimum insertion loss around 1.5 dB and maximum insertion loss at 3.6 dB in 83.5-MHz bandwidth, which is suitable for WLAN and Bluetooth applications. [DOI: 10.1117/1.2037387]

Subject terms: bulk acoustic device; inductive coupling plasma; MEMS resonator.

Paper 04174R received Dec. 10, 2004; revised manuscript received Feb. 2, 2005; accepted for publication Feb. 8, 2005; published online Aug. 30, 2005.

1 Introduction

Filters are critical components for wireless communication systems, especially in high frequency regions. Currently, most radio frequency filters involve surface acoustic wave (SAW) filters; however, the power handling capability is not adequate for certain applications. For example, the filters after the power amplifier and before the antenna in the transmitter stage must sustain high output powers to about 30 dBm. Most SAW filters specify safe input power of only around 10 dBm, lower than the requirement. Thin film bulk acoustic wave resonator (FBAR) technology utilizes bulk acoustic waves. It has features of high power handling capability, small size, and the possibility of further integration with semiconductor components. Therefore, FBAR is a promising solution for these filter applications.

Presently, the fabrication methods for FBARs can be classified into three categories: backside wet etching processes,[1,2] frontside etching processes,[3,4] and multilayer reflection methods,[5,6] as shown in Fig. 1. However, the multilayer reflection method requires thickness and stress control for each layer. It is difficult to precisely control the performance of the FBAR fabricated using the frontside etching process, since the selectivity cannot be ignored during bulk etching. The backside wet etching process has drawbacks of large device size and also has difficulties in frontside protection. Besides device fabrication, applications of FBAR[7,8] and materials suitable for FBAR have also been extensively investigated.[9,10] Nevertheless, device performance and design flexibility still highly depend on the predefined process. Therefore, a reliable fabrication process is expected.

In this study, a FBAR was demonstrated using a modified back-side etching process. The key idea was to employ inductive coupling plasma (ICP) to implement the backside etching process. Since high aspect ratio structures can be realized using the ICP etching process, devices with much smaller feature size can be fabricated. Moreover, ICP etching has the characteristics of a dry process and larger selectivity between substrate and films, and the protection of the front side during bulk etching. Resonators and filters were also fabricated and characterized to confirm the feasibility of this process design.

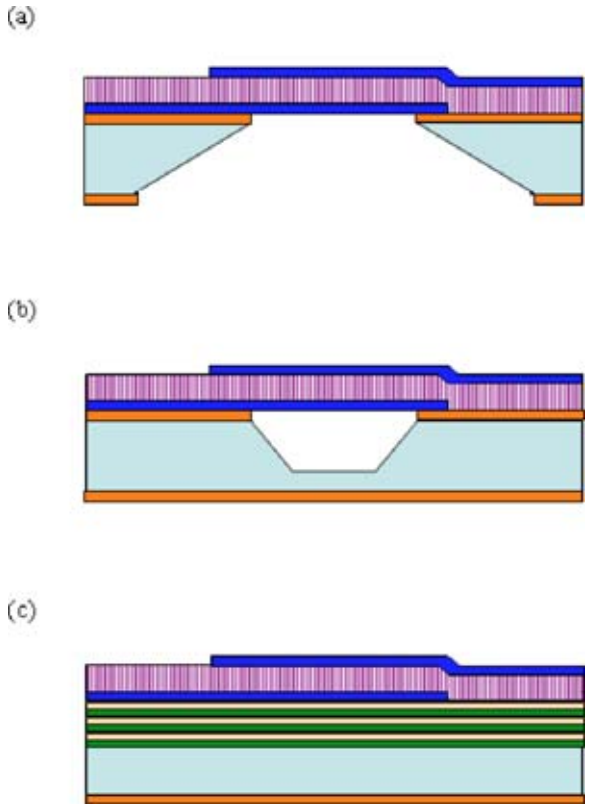

Fig. 1 Typical FBAR structures: (a) backside etched structure, (b) frontside etched structure, and (c) multilayer structure.

1537-1646/2005/$22.00

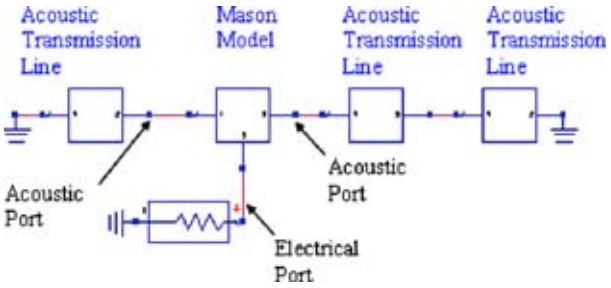

Fig. 2 Simulation schematic of a bulk acoustic resonator.

2 Design and Analysis

Thin film bulk acoustic resonators operate like quartz resonators, except that they are fabricated by thin film technology. Since the device geometry can be made extremely small, their operation frequency is much higher than that of quartz resonators. As shown in Fig. 1(a), a typical FBAR is a stacked structure consisting of a piezoelectric layer and two electrode layers. In addition, this stacked structure is suspended so that both the top and bottom surface are free to deform in out-of surface directions. The piezoelectric layer is used to generate longitudinal acoustic waves along the thickness direction. Since longitudinal acoustic waves perfectly reflect at free surfaces, e.g., a solid-air interface, standing waves can be created in the FBAR structure at desired frequencies. The piezoelectric film then transfers energy from acoustic standing waves to electrical resonance.

An accurate model is required to simulate the complex behavior of FBAR. In this work, an acoustic transmission line model was used.[11] This model treats all acoustic layer segments as microwave transmission lines using the force-voltage analogy. In addition, a conventional Mason equivalent circuit model was used for the modeling of piezoelectric materials. This model comprised two acoustic ports and one electrical port,[11] as shown in Fig. 2. The acoustic ports were connected to acoustic transmission lines to model propagations of acoustic wave in a multilayered structure. The electrical port could pass voltage and current information to nearby electrical circuits. By connecting Mason's equivalent circuit model and acoustic transmission line models in a series, frequency response of the stacked structure was simulated. The simulated resonance frequency of the proposed FBAR is around 2.4 GHz. Moreover, from the series resonance frequency f_s and parallel resonance frequency f_p, the electromechanical coupling coefficient (K^2) was expressed as,[12]

$$K^2 = \frac{\frac{\pi}{2}\frac{f_s}{f_p}}{\tan\left(\frac{\pi}{2}\frac{f_s}{f_p}\right)}. \quad (1)$$

A good resonator for filter application should have a wide separation between f_s and f_p, which represents a high electromechanical coupling coefficient (K^2). Higher K^2 facilitates wide band filter design and fabrication.

The relationship between resonance frequency, electromechanical coupling coefficient (K^2), and structure thickness was predicted using the aforementioned simulation model. The FBAR can be designed to operate at various resonance frequencies and electromechanical coupling coefficients for different combinations of piezoelectric layer, top electrode, and bottom electrode thicknesses. In this study, the thickness of the bottom electrode was fixed, and the effective electromechanical coupling coefficient K^2 was tuned by varying the thickness ratio of the piezoelectric layer to the top electrode layer. In general, to increase the coupling coefficient K^2 at a particular resonance frequency, the thickness ratio (TR) of a piezoelectric layer to the top electrode layer needs to be increased. Figure 3 shows typical simulation results of effective electromechanical coupling coefficients at different TRs of piezoelectric layers to top electrode layers. The simulation employed AlN as the piezoelectric layer, Ti-Pt as the bottom electrode layer, and Al as the top electrode layer. According to the simulation results in Fig. 3, the FBAR could achieve a better electromechanical coupling coefficient if the thickness ratio is greater than 5. However, the electrode thickness could not be too thin for the conductivity and thin-film deposition considerations (i.e., film thickness control). After compromising device performance and manufacturability, a favorable thickness combination, including the bottom electrode layer, piezoelectric layer, and top electrode layer, was selected for the following fabrication processes. The piezoelectric layer was around 2 μm, and the top and bottom electrodes are less than 4000Å.

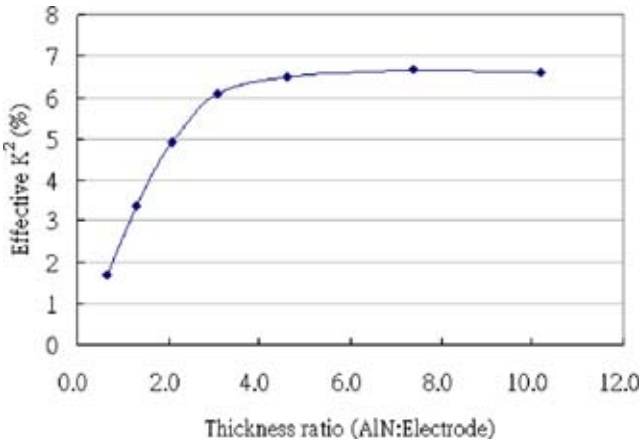

Fig. 3 Simulation result of effective electromechanical coupling coefficient at different piezoelectric layers to top electrode thickness ratio.

Conventional ladder-type filter design was used in this work.[13] As shown in Fig. 4, the filter in this study consists of seven resonators. These seven resonators were designed to have only two different resonant frequencies. Thus, the characteristics of the filter were determined by these two resonant frequencies of the resonators. In general, the design parameters of the filter included the planar dimensions, resonant frequency, and electromechanical coupling factor of the resonator. According to Mason's model, the information of resonance frequency and the electromechanical coupling coefficient can be simulated. Moreover, the quality factor of the resonator has already been determined during the deposition of the piezoelectric film. In this work, the quality factor Q_s was not be tuned by process means, it was

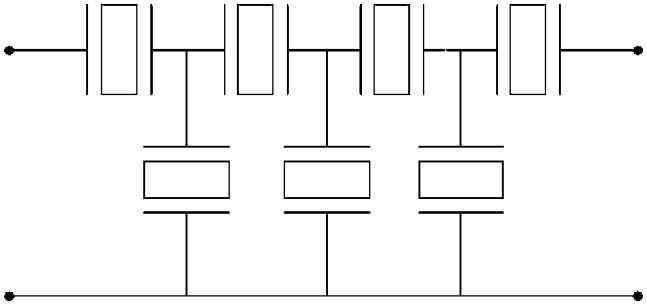

Fig. 4 Configuration of a typical ladder-type filter.

regarded as a fixed parameter during design. Consequently, the remaining parameters were the planar dimensions of the resonator, which directly affects the mask layout. A minimum-size filter was preferred. In addition, the filter designed in this study must meet the requirement of low insertion loss and high rejection. In summary, the desired filter has the following specifications: center frequency is 2441.75 MHz, bandwidth is 83.5 MHz, rejection is more than 25 dB, and return loss is greater than 10 dB. To this end, ADS commercial software was employed to design the planar dimensions of the device to optimize filter performance.[14] Since the thickness of the piezoelectric film was 2 μm, the optimal length of each resonator was in the range of 100 to 300 μm.

3 Fabrication Process and Results

The fabrication processes employed in this study are summarized in Fig. 5. As shown in Fig. 5(a), a silicon dioxide layer was thermally grown on a (100) silicon substrate, and then a silicon nitride layer was deposited on top of it. These two layers not only insulate devices from silicon substrate, but also act as etching stop layers for the ICP process. The bottom electrode was deposited and patterned, as shown in Fig. 5(b). After that, the piezoelectric layer was deposited and patterned, as illustrated in Fig. 5(c). Aluminum nitride (AlN) was selected in this process to be the piezoelectric layer. Since the AlN(002) structure grown on Pt has better orientation,[15] Ti-Pt film was employed as the material for the bottom electrode in Fig. 5(b). The dc sputtering process was used in Fig. 5(c) to deposit the AlN film, and the wafer temperature was 160 °C, which was measured by a thermal couple attached directly at the substrate. The AlN film was etched to provide connection between the bottom electrode and top electrode. According to the higher etching rate, wet chemical etching was preferred to pattern the AlN. Moreover, the slope of the sidewall could be tuned to about 1/20 by wet etching, as indicated in Fig. 5(c). Thus, the step coverage was significantly improved due to this inclined sidewall. Disconnection of the conducting metal wires caused by the step coverage problem was eliminated. After that, the top electrode was deposited and the geometry was defined by a lift-off process, as shown in Fig. 5(d). The material of the top electrode was aluminum, which has low resistively and low density as well. Since the FBAR filter should be comprised of resonators with two different frequencies, an additional thin metal layer was deposited on some of the resonators to shift down the resonance frequency as shown in Fig. 5(e). Afterward, backside bulk

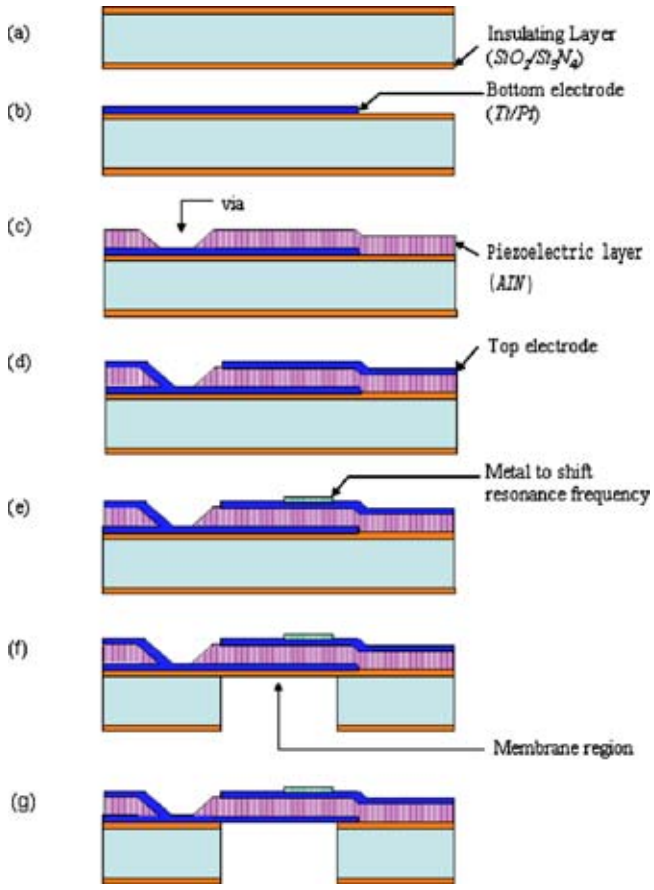

Fig. 5 FBAR fabrication process using backside ICP.

silicon etching was implemented using ICP, and then the thin membrane was formed, as shown in Fig. 5(f). The membrane was free at both top and bottom surfaces, therefore the resonator achieved a high quality factor. Finally, insulating layers (SiO_2 and Si_3N_4) under the membrane were removed to increase the quality factor and fine tune the resonance frequency, as shown in Fig. 5(g).

The fabricated devices were designed to have compact size 1×1 mm, therefore the total number of devices on the six-inch wafer was about 10,000. Figure 6(a) shows the top view photo of the fabricated filter. The in-plane dimensions of the filter cavity was about 430×550 μm. As indicated in Fig. 6(a), there are seven resonators with different sizes: the largest resonator was about 180×160 μm and the smallest resonator was about 120×150 μm. This photo also shows that the electrodes and FBAR membrane were not damaged during the backside etching process. The SEM photo in Fig. 6(b) shows the cross section view of a typical suspended FBAR filter. It is clearly observed from the SEM photo that the filter has vertical sidewalls perpendicular to the wafer surface. The experiment results demonstrated that the size of the filter was significantly reduced by the ICP etching process, compared with the backside wet etching process, which normally consumes a four times larger area due to anisotropic etching characteristics. In addition, the ICP etching was a dry process and had high material etching selectivity, so that this process could prevent material overetching and membrane sticking problems. These prob-

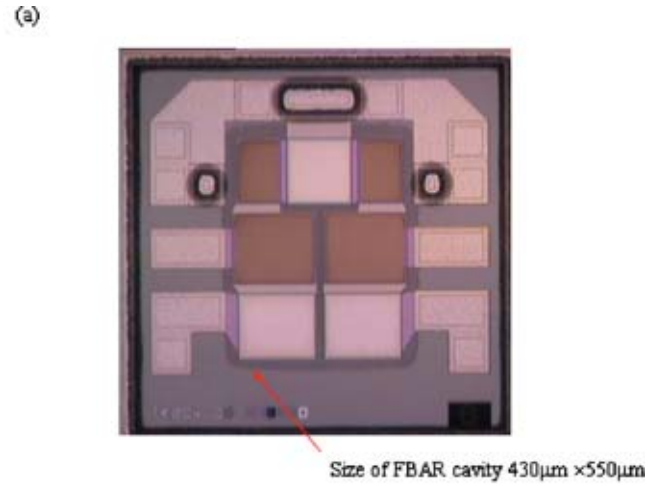

Fig. 6 Photos of the fabricated device: (a) top view and (b) cross section view.

lems frequently occur in existing FBAR fabrication methods.[1–4] Figure 7 shows the zoom-in photo of the membrane structure. It demonstrates that the micrometer-thick AlN film had grown well on the Ti-Pt film, therefore the collimated structure throughout the layer can be observed. Moreover, an x-ray diffraction XRD pattern was measured

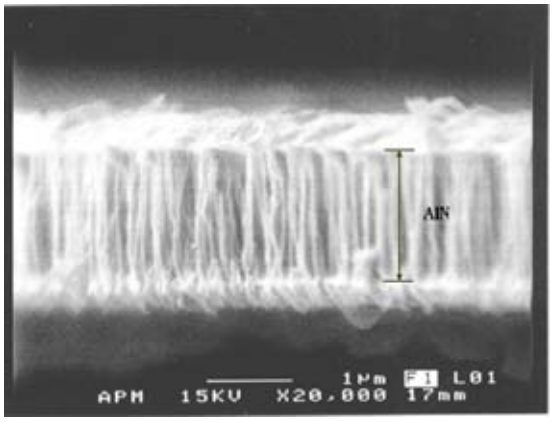

Fig. 7 Collimated structure of AlN can be identified in the suspended membrane.

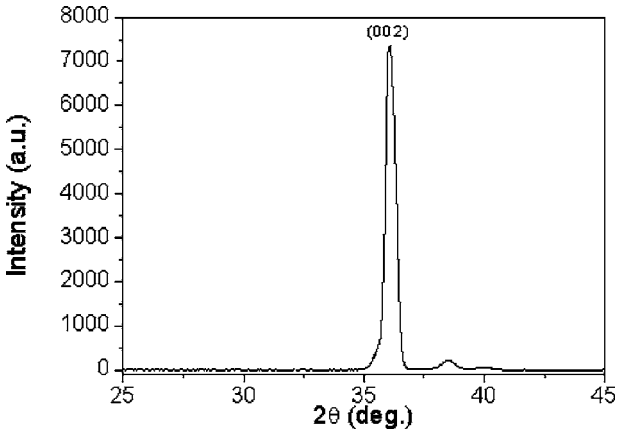

Fig. 8 XRD pattern of sputtered AlN film.

to demonstrate the orientation quality of AlN, as shown in Fig. 8. In this figure, an AlN (002) peak can be clearly observed at 36 deg. The packaged size can be 3×3 mm by wire bond method or 2.5×2.0 mm by flip chip method. This size is the same as that of SAW filters but is much smaller than that of ceramic filters.

4 Measurement and Results

To demonstrate the performance of the device fabricated using the processes in Fig. 5, two types of acoustic devices were measured. In addition to characterizing the performance of the filter, the resonator was employed as a test key to identify the quality factor of the device. During the test, both of these two devices were characterized by network analyzer and on-wafer probe sets. The overall measurement setup, included probes and lines, were calibrated using short-load-open-through impedance standard substrates at the beginning of the measurement.

Resonator test keys were tested by the one-port test method. Moreover, to demonstrate the overall performance of the resonator device, the parasitic resistance on the chip

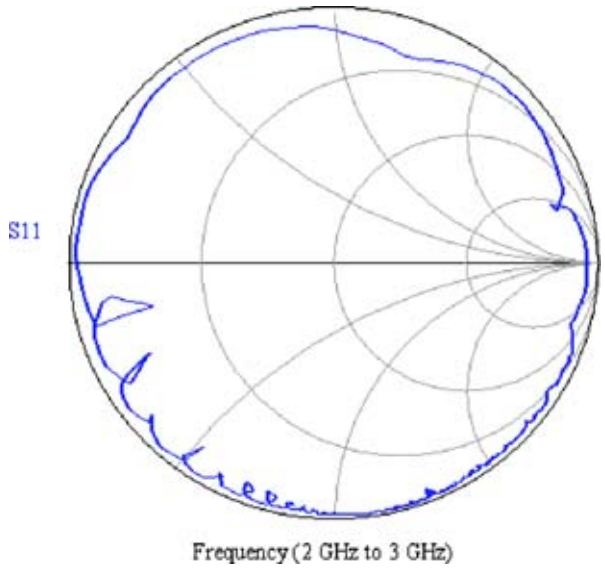

Fig. 9 Measured resonator characteristic in Smith chart form.

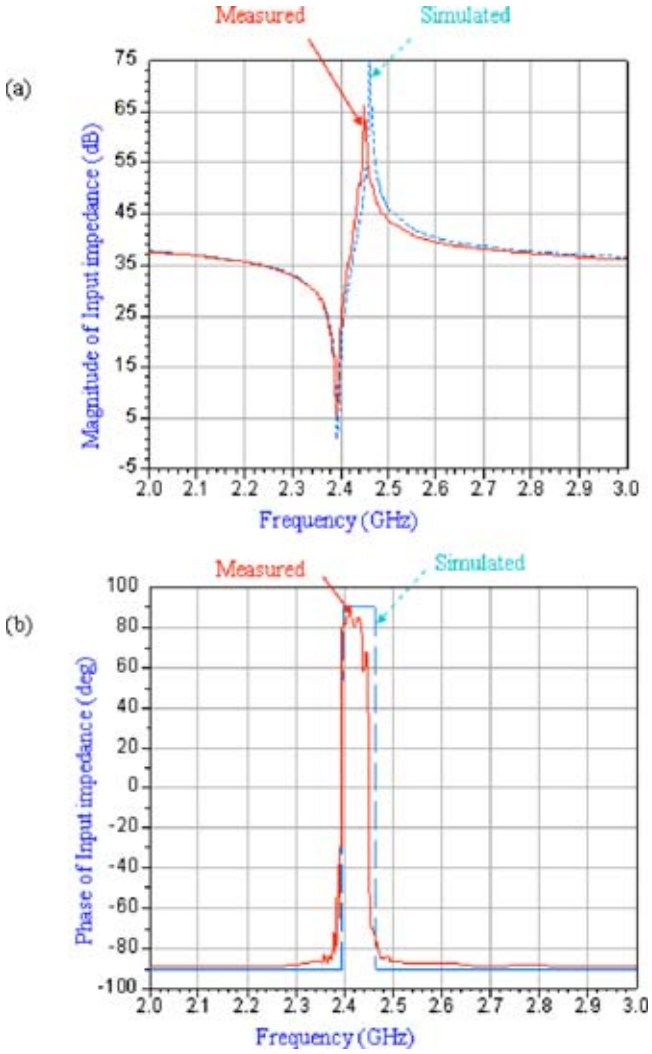

Fig. 10 Comparison of measured and simulated input impedances for (a) magnitude and (b) phase.

was not de-embedded after measurement. Test results of resonators are shown in Figs. 9 and 10. Figure 9 shows the S11 of the resonator in the form of a Smith chart. It shows that a very small effective series resistance was presented, so that the measured S11 circle was slightly shrunk. However, this small amount of series resistance in the resonator was acceptable for filter application purposes.

Figure 10(a) shows the measured and simulated magnitude of input impedance. The measured series resonance frequency f_s and the parallel resonance frequency f_p in Fig. 10(a) were determined by the minimum and maximum input impedance, respectively. According to the measured f_s and f_p, the electromechanical coupling coefficient (K^2) of this device extracted from Eq. (1) was about 5.7%. Simulation of the input impedance utilized transmission line model is described in Sec. 2. The simulation results agree well with the measured ones. However, the measured curve had a narrower separation of f_s and f_p than the simulated one. This is because the simulation model employed an ideal piezoelectric constant. Figure 10(b) shows the measured and simulated phase of input impedance. For an ideal

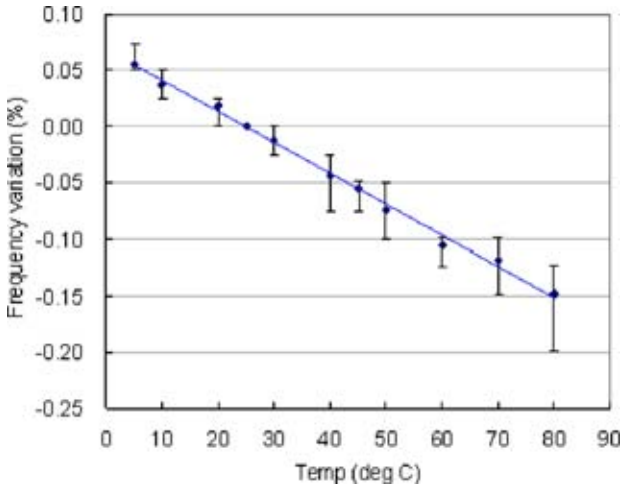

Fig. 11 Relationship between temperature and variation of resonance frequency.

resonator, the phase should change from −90 to +90 deg in steep slope at the series resonance and parallel resonance points. However, if the resonator had energy dissipation, the slope of phase change becomes gentle. The quality factor (Q_s) at the series resonance frequency was calculated by the rate of phase change with frequency at resonance[12]:

$$Q_s = \frac{f_s}{2}\left|\frac{d\angle Z_{in}}{df}\right|, \tag{2}$$

where $\angle Z_{\text{in}}$ is the phase of input impedance. For this device, the phase change was quite steep at the series resonance point, therefore the resonance had a very high quality factor. The quality factor at the series resonance point was calculated to be 1567 for this device. These electrical performances show that the ICP process was promising for the fabrication of bulk acoustic resonators.

The characteristics of resonators were sensitive to the ambient temperature.[4] In this regard, the resonators were also tested under various temperatures using the thermal chuck and wafer probing method. The temperature was controlled to rise from 25 to 80 °C and then cool down from 80 to 5 °C. Series resonance frequencies were recorded and plotted in Fig. 11, where each error bar represents five measurement data. The measured relationship between temperature and resonance frequency was linear. In addition, the temperature coefficient of resonance frequency was about −27.4 ppm/ °C, which was consistent with Ref. 4. After the device temperature cooled down from high temperature to room temperature, the resonance frequency returned to its original value at room temperature. These results indicated that although bulk acoustic wave devices using the ICP method consisted of a suspended structure, such as a membrane, they still held good thermal conductivity. Thus, there was no heat piled up in the device during temperature variation.

Next, the filter performance was measured. This filter was a traditional ladder-type design; it included four serially connected resonators and three shunt resonators. Figure 12 shows the typical measurement result. The minimum insertion loss was about 1.5 dB and maximum insertion

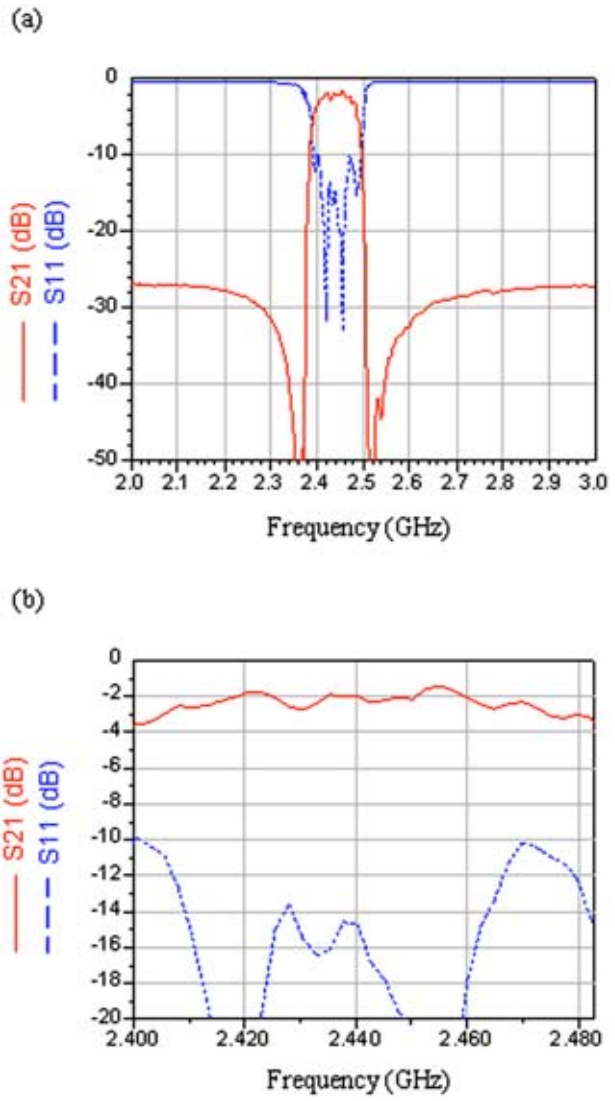

Fig. 12 Filter performance of (a) wide band and (b) narrow band.

loss in 83.5-MHz bandwidth was 3.6 dB. Moreover, the in-band return loss was more than 10 dB and the minimum out-of-band rejection was 25 dB. According to the test results, this high frequency filter had good electric performance comparable to SAW filters, which typically specify maximum insertion loss as 3.5 dB and rejection at 20 dB. Other frequency bands ranging from 1.5 to 2.2 GHz could be easily redesigned and fabricated by changing the electrode layout and thickness of suspended membranes.

5 Conclusion and Discussion

Thin film bulk acoustic resonators and filters are realized using ICP bulk silicon etching. Thus, the cavity on the silicon substrate after bulk etching has near vertical sidewalls. In this regard, the size of the devices is significantly reduced to 25% compared to wet etching processes. In addition, the performance of the devices is also properly controlled. A transmission line model is used to simulate the performance of the resonator. According to the simulation results, the preferable structure thickness is determined. The devices are tested by a network analyzer and probe station. The quality factor and electromechanical coupling coefficient of a single resonator are 1567 and 5.7%, respectively. The insertion loss of the filter in Fig. 11 has a maximum of 3.6 dB at 83.5-MHz band (from 2.4 to 2.4835 GHz). In addition, the rest of the region has more than 25-dB rejection. These fabrication and test results demonstrate that high-quality thin film bulk acoustic resonators and filters can be designed and fabricated using an ICP process.

As shown in Fig. 9, the measured resonator performance has some unwanted modes near the resonance points. These modes could result in unwanted ripples near the passband. To overcome this problem, resistive loss could be deliberately added in the cost of higher insertion loss. However, the required amount of resistance is hard to predict or simulated, therefore extensive experiments should be carried out.

Acknowledgment

The author would like to express his appreciation to Asia Pacific Microsystems, Incorporated (Taiwan) for providing fabrication facilities and technical assistance.

References

1. S. V. Krishnaswamy, J. Rosenbaum, S. Horwitz, C. Vale, and R. A. Moore, "Film bulk acoustic wave resonator technology," in *Proc. IEEE Ultrasonics Symp.*, pp. 529–536, Honolulu, HI (Dec. 1990).
2. J. Y. Park, H. C. Lee, K. H. Lee, H. M. Lee, and Y. J. Ko, "Micromachined FBAR RF filters for advanced handset applications," in *IEEE Intl. Conf. Solid State Sensors, Actuators and Microsyst.*, pp. 911–914, Boston, MA (June 2003).
3. R. Ruby, P. Bradley, J. D. Larson III, and Y. Oshmyansky, "PCS 1900 MHz duplexer using thin film bulk acoustic resonator (FBARS)," *Electron. Lett.* **35**, 794–795 (1999).
4. J. D. Larson III, R. C. Ruby, P. D. Bradley, J. Wen, S. L. Kok, and A. Chien, "Power handling and temperature coefficient studies in FBAR duplexers for the 1900 MHz PCS band," in *2000 IEEE Ultrasonics Symp.*, Vol. 1, pp. 869–874, San Juan, Puerto Rico (2000).
5. K. M. Lakin, K. T. McCarron, and R. E. Rose, "Solidly mounted resonators and filters," in *Proc. IEEE Ultrasonics Symp.*, pp. 905–908, Seattle, WA (Nov. 1995).
6. G. Yoon and J. D. Park, "Fabrication of ZnO-based film bulk acoustic resonator devices using W/SiO2 multilayer reflector," *Electron. Lett.* **36**, 1435–1437 (2000).
7. R. Ruby, P. Bradley, D. Clark, D. Feld, T. Jamneala, and K. Wang, "Acoustic FBAR for filters, duplexers and front end modules," in *2004 IEEE MITT-S Int. Microwave Symp. Digest*, pp. 931–934, Fort Worth, TX (June 2004).
8. A. P. S. Khanna, E. Gane, and T. Chong, "A 2GHz voltage tunable FBAR oscillator," in *2003 IEEE MTT-S Int. Microwave Symp. Digest*, Vol. 2, pp. 717–720, Philadelphia, PA (June 2003).
9. J. P. Jung, J. B. Lee, M. H. Lee, and J. S. Park, "Experimental and theoretical investigation on the relationship between AlN properties and AlN-based FBAR characteristics," in *Proc. Ann. IEEE Intl. Frequency Control Symp.*, pp. 779–784, Tampa, FL (May 2003).
10. T. Y. Kang, M. J. Keum, I. H. Son, K. S. Kim, J. B. Lee, and K. H. Kim, "Preparation of AZO/ZnO/AZO/SiO_2/Si thin film for FBAR," in *2003 IEEE Ultrasonics Symp. Proc.*, pp. 2016–2019, Honolulu, HI (Oct. 2003).
11. B. A. Auld, *Acoustic Fields and Waves in Solids*, John Wiley and Sons, New York (1973).
12. K. M. Lakin, "Modeling of thin film resonators and filters," in *Digest IEEE Microwave Symp.*, pp. 149–152, Albuquerque, NM (June 1992).
13. K. M. Lakin, G. R. Kline, and K. T. McCarron, "Thin film bulk acoustic wave filters for GPS," in *Proc. IEEE Ultrasonics Symp.*, pp. 471–476, Tucson, AZ (Dec. 1992).
14. J. D. Larson III, R. Ruby, P. Bradley, and Y. Oshmyansky, "A BAW antenna duplexer for the 1900 MHz PCS band," in *Proc. IEEE Ultrasonics Symp.*, pp. 887–890, Caesars Tahoe, NV (Oct. 1999).
15. H. P. Lobl, M. Klee, R. Milsom, R. Dekker, C. Metzmacher, W. Brand, and P. Lok, "Materials for bulk acoustic wave (BAW) resonators and filters," *J. Eur. Ceram. Soc.* **21**, 2633–2640 (2001).

Chung-Hsien Lin received his MS degree from National Tsing Hua University in 1999. From 2001 to 2004, he worked as a design engineer in Asia-Pacific Microsystems, Incorporated, Taiwan. His job duties focused on the design and fabrication of RF-MEMS components. He is currently a PhD student in the power mechanical engineering department at National Tsing Hua University. His research interests include MEMS with emphasis on RF-MEMS, CMOS-MEMS, and microsensors.

Hong-Ren Chen received his BS degree in marine engineering from National Taiwan Ocean University in 1993. He got the MS and PhD degrees from the Institute of Aeronautics and Astronautic from National Cheng Kung University, Taiwan, in 1995 and 2001, respectively. He has been working as a section manager in the wireless system division of Asia Pacific Microsystems, Incorporated, Hsinchu, Taiwan, since 2001. His research interests include design and fabrication of microfluidic systems and RF MEMS devices, microscale flow, and heat transfer.

Weileun Fang received his PhD degree from Carnegie Mellon University in 1995. His doctoral research focused on determining the mechanical properties of thin films using micromachined structures. In 1995, he worked as a postdoctoral research fellow at Synchrotron Radiation Research Center, Taiwan. He is currently a professor in the power mechanical engineering department at National Tsing Hua University, Taiwan. His research interests include MEMS with emphasis on micro-optical systems, microactuators, and the characterization of the mechanical properties of thin films.